Geophys. J. Int. (2000) **142,** 000–000

Superiority of Optimally Accurate Schemes for Numerical Calculation of Synthetic Seismograms: 1-D Examples

Nobuyasu Hirabayashi[1], Robert J. Geller[2] and Hiromitsu Mizutani[3]

[1] *Sclumberger Oilfield Services, 10001 Richmond, Houston, TX 77042, USA. E-mail: nhirabayashi@slb.com, and Dept. of Earth and Planetary Science, Graduate School of Science, University of Tokyo, Hongo 7-3-1, Bunkyo-ku, Tokyo 113-0033 Japan*

[2] *Dept. of Earth and Planetary Science, Graduate School of Science, University of Tokyo, Hongo 7-3-1, Bunkyo-ku, Tokyo 113-0033 Japan. E-mail: bob@eps.s.u-tokyo.ac.jp*

[3] *Institute for Frontier Research on Earth Evolution (IFREE), Japan Agency of Marine-Earth Science and Technology (JAMSTEC), 3173-25 Showa-machi, Kanazawa-ku, Yokohama, Kanagawa, 236-0001, Japan. E-mail: miju@jamstec.go.jp*

SUMMARY

Optimally accurate $O(2,2)$ — second order in time and space — time domain finite difference method (FDM) schemes have previously been derived on the basis of the general criterion for optimally accurate numerical operators of Geller & Takeuchi (1995) and have been shown to significantly outperform conventional $O(2,2)$ FDM schemes. In this paper we use this criterion to derive two new optimally accurate schemes: an $O(2,4)$ — second order in time and fourth order in space — time domain FDM scheme, and a scheme using the spectral element method (SEM) as the spatial operator and second order FDM as the temporal operator. In each case the performance of the optimally accurate scheme is greatly superior to the corresponding conventional scheme, while the performance of the various optimally accurate schemes is roughly comparable. Only one-dimensional (1-D) test cases are considered, in this paper, but the conclusions of this study is also applicable to 2-D and 3-D cases.

1 INTRODUCTION

Analyses of seismic data to determine earth structure and seismic source parameters require accurate and efficient methods for computing synthetic seismograms. Many methods are available for computing synthetics, and users would like to know which method is “best”. This question does not necessarily have a single simple answer, because the accuracy and efficiency of such methods depend both on the nature of the problem and the computational equipment being used. Nevertheless this question obviously has great practical importance, because full waveform methods are becoming an increasingly important data analysis tool in both forward modeling and inverse studies.

Practical applications will almost always utilize complex heterogeneous models, but the simple numerical examples presented in this paper provide insight into the comparative advantages and disadvantages of various methods. Only time domain schemes are considered in this paper. Generally speaking, time domain methods are preferable for problems requiring broad-band synthetics for a short time duration, whereas frequency domain methods are preferable for long time durations and relatively narrow bandwidth. However a detailed comparison of time domain and frequency domain methods is outside the scope of this paper.

All purely numerical schemes for computation of synthetic seismograms discretize the elastic equation of motion. Several widely used schemes are based on the finite difference method (FDM). Other schemes use the pseudo-spectral method (PSM) or the spectral element method (SEM) to compute spatial derivatives. The goal of this paper is to compare the cost-effectiveness of different methods, but before we do this we must first ensure that the numerical scheme for each of the methods being tested is as efficient as possible for a method of that type.

Historically, numerical schemes were evaluated using the numerical dispersion of the phase velocity as the accuracy criterion, but this can be evaluated only for a homogeneous medium. In this paper we follow Geller & Takeuchi (1995), and Geller & Takeuchi (1998), hereafter referred to respectively as GT95 and GT98, in using the relative error of the synthetic seismograms (defined by eq. 49, below) as the metric for quantifying the error of the synthetics, since this can be applied to an arbitrarily heterogeneous medium.

GT95 derived a general criterion for optimally accurate operators that can be applied to arbitrarily heterogeneous media. This criterion was applied by GT98 and Takeuchi & Geller (2000) to derive optimally accurate time domain FDM schemes that are second order in space and time, usually referred to as O(2,2). These papers showed that optimally accurate O(2,2) FDM schemes have a significantly better cost-performance ratio than conventional (non-optimally accurate) O(2,2) FDM schemes.

In this paper we use the criterion of GT95 to derive an optimally accurate $O(2,4)$ time domain FDM scheme (2nd order in time and 4th order in space), and an optimally accurate scheme with an SEM spatial operator and with a second order FDM temporal operator. We then compare the performance of the new optimally accurate schemes to the corresponding conventional schemes, and show that the former are superior. Finally, we compare the performance of the three optimally accurate schemes.

Displacement is the only dependent variable in the schemes considered in this paper. In contrast, 'staggered grid' FDM schemes use displacement and stress (or velocity and the time derivative of stress) as coupled dependent variables. However, Geller *et al*. (2005a) showed that staggered grid FDM schemes can be transformed to rigorously equivalent non-optimally accurate one-step FDM schemes whose performance is slightly inferior to conventional one-step FDM schemes. Thus it is unnecessary to consider staggered grid methods in this paper.

The outcome of a comparison of numerical schemes can depend on whether a homogeneous or heterogeneous medium is being used as the test case. For example, some authors tested PSM schemes for a homogeneous medium and reported that they outperformed FDM. However, Mizutani *et al*. (2000) showed that for a simple heterogeneous medium with sharp lithological discontinuities the optimally accurate $O(2,2)$ FDM scheme outperformed an optimally accurate PSM scheme. Since geophysicists are interested in applying numerical calculations to the actual Earth, which is of course highly heterogeneous, we emphasize results for heterogeneous test models in the present paper, although we also present some results for a homogeneous model. On the basis of the conclusions of Mizutani *et al*. (2000), we exclude the PSM from consideration.

2 NUMERICAL SCHEMES

In this paper, for simplicity, we consider only the 1-D case, but the general approach followed here can also be applied to the 2-D and 3-D cases. The strong form of the elastic equation of motion (see Geller & Ohminato, 1994) for the 1-D case in the time domain is as follows:

$$\rho(x)\frac{\partial^2 u(x,t)}{\partial t^2} - \frac{\partial}{\partial x}\left(\mu(x)\frac{\partial u(x,t)}{\partial x}\right) = f(x,t), \tag{1}$$

where ρ is the density, μ is the rigidity, u is the displacement, and f is the external body force. We solve this equation numerically using the various schemes discussed below. All of the FDM schemes used in this paper automatically satisfy free surface external boundary conditions and continuity of traction at internal boundaries, as they are natural boundary conditions (see Geller & Ohminato 1994 for details).

2.1 Optimally Accurate FDM Schemes

The optimally accurate $O(2,2)$ time domain FDM scheme used in this study is that of GT98. Both one-step and staggered-grid non-optimally accurate $O(2,4)$ FDM schemes have been widely published (e.g., Levander 1988; Robertsson 1994; Cohen & Joly 1996) but, as an optimally accurate $O(2,4)$ scheme has not been previously derived, we now do this. We also derive both conventional and optimally accurate operators for a free surface or an internal lithological discontinuity.

Our basic approach to deriving the optimally accurate $O(2,4)$ scheme parallels GT98's (pp. 49-53) approach to deriving the optimally accurate $O(2,2)$ FDM scheme. We begin by deriving results for the case of a homogeneous medium in some detail, and then we present a summary of key results for the case of a medium where the density and elastic properties vary with spatial position.

Following GT98, we write the conventional one-step $O(2,4)$ FDM scheme for the elastic equation of motion (eq. 1) in the following operator form:

$$(\mathbf{A^0} - \mathbf{K^0})\mathbf{c} = \mathbf{f}, \tag{2}$$

where $\mathbf{A^0}$ is the conventional second order FDM operator for $\rho(\partial^2 u/\partial t^2)$, $\mathbf{K^0}$ is the conventional fourth order FDM operator for $\partial/\partial x[\mu(\partial u/\partial x)]$, $\mathbf{c}$ is the displacement vector and $\mathbf{f}$ is the discretized external force.

As is well known, the difference stencils at interior points for the conventional $O(2,4)$ FDM operators are as follows:

$$\mathbf{A^0} = \frac{\rho}{\Delta t^2} \times$$

	$x-2\Delta x$	$x-\Delta x$	x	$x+\Delta x$	$x+2\Delta x$
$t-\Delta t$			1		
t			-2		
$t+\Delta t$			1		

(3)

$$\mathbf{K^0} = \frac{\mu}{12\Delta x^2} \times$$

	$x-2\Delta x$	$x-\Delta x$	x	$x+\Delta x$	$x+2\Delta x$
$t-\Delta t$					
t	-1	16	-30	16	-1
$t+\Delta t$					

(4)

We now follow the same basic steps as GT98's derivation of the optimally accurate $O(2,2)$ scheme to derive the stencils for the optimally accurate $O(2,4)$ operators. The optimally accurate scheme is written

$$(\mathbf{A}-\mathbf{K})\mathbf{c} = \mathbf{f}, \tag{5}$$

where **A** is the optimally accurate second order FDM operator for $\rho(\partial^2 u/\partial t^2)$, **K** is the optimally accurate fourth order FDM operator for $\partial/\partial x[\mu(\partial u/\partial x)]$, **c** is the displacement vector and **f** is the discretized external force. We evaluate the errors of the respective conventional operators, and then "smear" the temporal operator in space and the spatial operator in time, so that the respective errors cancel. The optimally accurate operators **A** and **K** at interior points are written respectively as

$$\mathbf{A} = \frac{\rho}{90\Delta t^2} \times$$

	$x-2\Delta x$	$x-\Delta x$	x	$x+\Delta x$	$x+2\Delta x$
$t-\Delta t$	-1	4	84	4	-1
t	2	-8	-168	-8	2
$t+\Delta t$	-1	4	84	4	-1

(6)

and

$$\mathbf{K} = \frac{\mu}{144\Delta x^2} \times$$

	$x-2\Delta x$	$x-\Delta x$	x	$x+\Delta x$	$x+2\Delta x$
$t-\Delta t$	-1	16	-30	16	-1
t	-10	160	-300	160	-10
$t+\Delta t$	-1	16	-30	16	-1

. (7)

If we used the operators in eqs. (6) and (7) as written, we would have an implicit scheme. To obviate this necessity, following GT98 (p. 53), we break the optimally accurate scheme into the following predictor-corrector scheme, where the conventional operators in eqs. (3) and (4) are the predictor, and the residuals (the difference between the operators in eqs. (6) and (7) and those in eqs. (3) and (4) are the corrector:

Predictor: $(\mathbf{A^0} - \mathbf{K^0})\mathbf{c^0} = \mathbf{f}$ (8)

Corrector: $(\mathbf{A^0} - \mathbf{K^0})\delta\mathbf{c} = -(\delta\mathbf{A} - \delta\mathbf{K})\mathbf{c^0}$ (9)

Update: $\mathbf{c} = \mathbf{c^0} + \delta\mathbf{c}$ (10)

where

$$\delta\mathbf{A} = \mathbf{A} - \mathbf{A^0}, \tag{11}$$

$$\delta\mathbf{K} = \mathbf{K} - \mathbf{K^0}. \tag{12}$$

We now derive the operator for the boundaries (either an external free surface or an internal lithological discontinuity). We assume that the boundary coincides exactly with a node of the numerical grid. For the case of a free surface at $x = 0$ we write the conventional fourth order spatial operator as the following "stiffness matrix",

$$\mathbf{H} = \frac{\mu}{12\Delta x^2} \times \begin{pmatrix} P & Q & -1 & & & & \\ Q & R & 16 & -1 & & & \\ -1 & 16 & -30 & 16 & -1 & & \\ & -1 & 16 & -30 & 16 & -1 & \\ & & \ddots & \ddots & \ddots & \ddots & \ddots \end{pmatrix}, \tag{13}$$

where the unknown parameters P, Q and R are determined as discussed below.

Our derivation (below) basically follows the procedure of GT95 (pp. 463-464). As shown in eq. (13), we use the full 5 point difference operator at interior nodes, but we lack sufficient columns and rows to use the full 5 point operator at the boundary node (the first row and column) and the node immediately adjacent to it (the second row and column). Thus the order of accuracy of the operator at the boundary and immediately adjacent node will be less than fourth order.

Note, however, that the existence of a boundary error in the operator eq. (13) does not mean that the solution at the boundary will be less accurate than at interior nodes. This is because the solution error is proportional to the eigenfunctions of the normal modes (See pp. 451-453 and Fig. 8 of GT95). We confirm this fact below through a numerical experiment.

There are only three unknowns in eq. (13) because **H** must be symmetric. We determine these unknowns as follows. First, we require the elements of each row to sum to zero, as the operator should not have any zero order contribution. We thus require:

$$P+Q-1=0, \tag{14}$$

$$Q+R+15=0. \tag{15}$$

We also require the Δx-dependent boundary term at $x=0$ to satisfy the following condition:

$$\frac{1}{12}[Pu(0)+Qu(\Delta x)-u(2\Delta x)]=\Delta x u'(0)+O(\Delta x^2). \tag{16}$$

Using a Taylor series expansions of the terms in eq. (16), we thus require:

$$Q-2=12. \tag{17}$$

Solving eqs. (14), (15) and (17) yields

$$P=-13,\ Q=14 \text{ and } R=-29. \tag{18}$$

We can also use the matrix operator (13) at internal sharp lithological boundaries, by "overlapping" the operators as shown in Fig. 3 of GT95.

Using eq. (13) with the above values of P, Q and R, together with the second order conventional

temporal operator (eq. 22 of GT98, p. 52), we follow the same general approach as GT98 to obtain the following stencils for the conventional spatial and temporal operators at the boundary ($x = 0$):

$$\mathbf{A^0} = \frac{\rho}{2\Delta t^2} \times$$

	x	$x+\Delta x$	$x+2\Delta x$
$t-\Delta t$	1		
t	-2		
$t+\Delta t$	1		

(19)

$$\mathbf{K^0} = \frac{\rho}{12\Delta x^2} \times$$

	x	$x+\Delta x$	$x+2\Delta x$
$t-\Delta t$			
t	-13	14	-1
$t+\Delta t$			

(20)

and at the adjacent point ($x = \Delta x$):

$$\mathbf{A^0} = \frac{\rho}{\Delta t^2} \times$$

	$x-\Delta x$	x	$x+\Delta x$	$x+2\Delta x$
$t-\Delta t$		1		
t		-2		
$t+\Delta t$		1		

(21)

and

$$\mathbf{K^0} = \frac{\rho}{12\Delta x^2} \times$$

	$x-\Delta x$	x	$x+\Delta x$	$x+2\Delta x$
$t-\Delta t$				
t	14	-29	16	-1
$t+\Delta t$				

. (22)

Following the same procedures as in eqs. (13) through (17), we derive the “mass matrix” for the boundary node and immediately adjacent node. As in the case of eq. (13) there are three unknowns (we again require symmetry). Omitting details, the final result is:

$$\mathbf{T} = \frac{\rho}{90} \times \begin{pmatrix} 44 & 2 & -1 & & & & \\ 2 & 85 & 4 & -1 & & & \\ -1 & 4 & 84 & 4 & -1 & & \\ & -1 & 4 & 84 & 4 & -1 & \\ & & \ddots & \ddots & \ddots & \ddots & \ddots \end{pmatrix} \tag{23}$$

Note that the derivation of the above results is similar to the derivation of of eq. (43) of GT98 (p. 55).

Using eqs. (13), (18) and (23), the stencils for the optimally accurate operators at the boundary ($x = 0$) and the immediately adjacent point ($x = \Delta x$) are as follows. At the boundary we have:

$$\mathbf{A} = \frac{\rho}{90\Delta t^2} \times$$

	x	$x+\Delta x$	$x+2\Delta x$
$t-\Delta t$	44	2	-1
t	-88	-4	2
$t+\Delta t$	44	2	-1

(24)

and

$$\mathbf{K} = \frac{\mu}{144\Delta x^2} \times$$

	x	$x+\Delta x$	$x+2\Delta x$
$t-\Delta t$	-13	14	-1
t	-130	140	-10
$t+\Delta t$	-13	14	-1

. (25)

At the adjacent point we have

$$\mathbf{A} = \frac{\rho}{90\Delta t^2} \times$$

	$x-\Delta x$	x	$x+\Delta x$	$x+2\Delta x$
$t-\Delta t$	2	85	4	-1
t	-4	-170	-8	2
$t+\Delta t$	2	85	4	-1

(26)

and

$$\mathbf{K} = \frac{\mu}{144\Delta x^2} \times$$

	$x-\Delta x$	x	$x+\Delta x$	$x+2\Delta x$
$t-\Delta t$	14	-29	16	-1
t	140	-290	160	-10
$t+\Delta t$	14	-29	16	-1

. (27)

2.2 Optimally accurate schemes for heterogeneous media

Optimally accurate $O(2,2)$ FDM operators for a 1-D medium with a spatially variable elastic constant and density have been given by GT98. We now derive optimally accurate $O(2,4)$ FDM operators for such a medium. We start with the conventional $O(2,4)$ FDM operators for interior points of a 1-D medium with a spatially variable elastic constant and density, given by Cohen & Joly (1996). The stencil for the temporal operator is given by eq. (3), above, except that ρ in eq. (3) is the value of the density at each particular node, while the stencil for the spatial operator is as follows:

$$\mathbf{K}^0 = \frac{1}{24\Delta z^2} \times \tag{28}$$

	$z-2\Delta z$	$z-\Delta z$	z	$z+\Delta z$	$z+2\Delta z$
$t-\Delta t$					
t	$-(\mu_0+\mu_{--})$	$16(\mu_0+\mu_-)$	$-16(\mu_-+2\mu_0+\mu_+)$ $+(\mu_{--}+2\mu_0+\mu_{++})$	$16(\mu_0+\mu_+)$	$-(\mu_0+\mu_{++})$
$t+\Delta t$					

,

where μ_{--}, μ_-, μ_0, μ_+ and μ_{++} are respectively the values of the elastic modulus at $x-2\Delta x$, $x-\Delta x$, …, $x+2\Delta x$. The optimally accurate temporal operator for the predictor step is given by eq. (6), except that the density ρ must be replaced by ρ_n, the displacement at each node point. The optimally accurate spatial operator for the predictor step is obtained from eq. (24) in the same way that eq. (7) is obtained from eq. (4), but its explicit form is not given here. A "numerical recipe" for the $O(2,4)$ optimally accurate predictor-corrector scheme is given in Appendix A.

We now follow the same approach used above to derive the stiffness matrix for the homogeneous medium with a free surface (see eqs. 13–18, above). Omitting intermediate steps, the first three rows of the stiffness matrix for the boundary elements are

$$H = \frac{1}{24\Delta z^2}\begin{bmatrix} H_{11} & H_{12} & H_{13} & & \\ H_{12} & H_{22} & H_{23} & H_{24} & \\ H_{13} & H_{23} & H_{33} & H_{34} & H_{35} \end{bmatrix} \tag{29}$$

where

$$H_{11} = -14(\mu_0+\mu_1)+(\mu_0+\mu_2) \tag{30}$$

$$H_{12} = 14(\mu_0+\mu_1) \tag{31}$$

$$H_{13} = -(\mu_0+\mu_2) \tag{32}$$

$$H_{22} = -14(\mu_0+\mu_1)-16(\mu_1+\mu_2)+(\mu_1+\mu_3) \tag{33}$$

$$H_{23} = 16(\mu_1+\mu_2) \tag{34}$$

$$H_{24} = -(\mu_1+\mu_3) \tag{35}$$

$$H_{33} = -16(\mu_1+2\mu_2+\mu_3)+(\mu_0+2\mu_2+\mu_4) \tag{36}$$

$$H_{34} = 16(\mu_2+\mu_3) \tag{37}$$

$$H_{35} = -(\mu_2+\mu_4) \tag{38}$$

and where the order of subscripts beneath the diagonal has been reversed because the matrix is symmetric. Note that the first row and column of H refer to the 0th node (at $x = 0$, with elastic modulus μ_0), the second row and column to the first node (at $x = \Delta x$, with elastic modulus μ_1), and so on.

Similarly, by following steps analogous to the derivation of eq. (23), we find that the first three rows of the mass matrix for the optimally accurate temporal operators for the heterogeneous case are as follows:

$$\mathbf{T} = \frac{1}{90}\begin{bmatrix} 44\rho_0 & 2\rho_0 & -\rho_0 & & \\ 2\rho_1 & 85\rho_1 & 4\rho_1 & -\rho_1 & \\ -\rho_2 & 4\rho_2 & 84\rho_2 & 4\rho_2 & -\rho_2 \end{bmatrix}. \tag{39}$$

The above matrix is not symmetric. As discussed on p. 460 of GT95 we could instead replace the matrix in eq. (39) by its symmetric part, but in practice the use of eq. (39) does not appear to cause any serious problems.

We do not give explicit results for the stencils for the boundary and the adjacent node, but the stencils for the conventional operators may be found in the same basic way as for eqs. (19)–(22), and those for the optimally accurate case in the same way as for eqs. (24)–(27).

2.3 Optimally Accurate SEM

The spatial operators for SEM schemes are well known (e.g., Komatitisch & Violotte 1998; Cohen 2002). In this study our SEM spatial operator follows Komatitsch & Tromp (1999). However, if second order FDM is used for the temporal operator, the standard treatment is not optimally accurate. We now derive an optimally accurate SEM scheme using 2nd order FDM time stepping, as follows. Except that the spatial operator uses SEM rather PSM, our derivation follows Mizutani *et al*. (2000, pp. 77-82), so we only present a brief summary here.

By using Lagrange polynomials as the weight functions and Gauss-Lobatto-Legendre numerical integration, the mass matrix for the weak form of eq. (1) becomes diagonal. Therefore the SEM equation can be written in the form

$$\frac{\partial^2 u}{\partial t^2} = \int_{\Omega} rhs\,(\partial u/\partial x, f)\,dx \tag{40}$$

where Ω denotes an element and $rhs(\partial u/\partial x, f)$ is a function of $\partial u/\partial x$ and $f(x,t)$. As we can assume that the spatial operator error of SEM is negligible, the right hand side of eq. (40) can be written as

$$RHS(x_i,t) = \sum_{j=1}^{l} \left(c_{ij}u(x_j,t) + d_{ij}f(x_j,t)\right) \tag{41}$$

where i is a node index of the model, l is a number of node points in an element, j is a node index in an element for numerical integration and c_{ij} and d_{ij} are coefficients. Using the conventional second order time difference operator, eq. (40) is written as follows:

$$\frac{u(x_i,t-\Delta t) - 2u(x_i,t) + u(x_i,t+\Delta t)}{\Delta t^2} = RHS(x_i,t) + \frac{1}{12}\frac{\partial^2}{\partial t^2}[RHS(x,t)] + O(\Delta t^4). \tag{42}$$

To derive an optimally accurate time-stepping scheme for SEM we follow basically the same

approach as Mizutani *et al.* (2000, pp. 77-80). To eliminate the second order error, we use the following relation:

$$\begin{aligned} & \frac{10}{12}RHS(x_i,t)+\frac{1}{12}\Big[RHS(x_i,t-\Delta t)+RHS(x_i,t+\Delta t)\Big] \\ = \;& RHS(x_i,t)+\frac{1}{12}\frac{\partial^2}{\partial t^2}[RHS(x,t)]+O(\Delta t^4). \end{aligned} \tag{43}$$

We now use eq. (43) to obtain an implicit optimally accurate SEM scheme as follows:

$$\begin{aligned} & \frac{u(x_i,t-\Delta t)-2u(x_i,t)+u(x_i,t+\Delta t)}{\Delta t^2} \\ = \;& \frac{10}{12}RHS(x_i,t)+\frac{1}{12}\Big[RHS(x_i,t-\Delta t)+RHS(x_i,t+\Delta t)\Big]+O(\Delta t^4). \end{aligned} \tag{44}$$

To obtain an explicit scheme for the above equation, the following predictor-corrector scheme is derived:

Step 1 (Predictor):

$$\hat{u}(x_i,t+\Delta t)=RHS(x_i,t)\Delta t^2-u(x_i,t-\Delta t)+2u(x_i,t) \tag{45}$$

Step 2 (Evaluation of Correction Term):

$$\delta u(x_i)=R\hat{H}S(x_i,t+\Delta t)\Delta t^2 \tag{46}$$

Step 3 (Update):

$$u(x_i,t+\Delta t)=\hat{u}(x_i,t+\Delta t)+\delta u(x_i) \tag{47}$$

where $\hat{u}(x_i,t+\Delta t)$ is the predictor of $u(x_i,t+\Delta t)$, $\delta u(x_i)$ is the corrector and

$$R\hat{H}S(x_i,t+\Delta t)=\sum_{j=1}^{l}\left(c_{ij}\hat{u}(x_j,t+\Delta t)+d_{ij}f(x_j,t+\Delta t)\right). \tag{48}$$

Several works using PSM schemes use fourth-order Runge-Kutta (RK4) rather than second order FDM as the temporal scheme. We also present numerical results for such PSM-RK4 schemes in the next section. As the details are basically the same as for PSM-RK4 (Mizutani *et al.* 2000, pp. 82-83), we omit details here.

3 NUMERICAL EXAMPLES

In this section we present one-dimensional numerical examples to compare the cost-effectiveness of the following FDM and SEM schemes:

(a) *Second order in space and time FDM*: a conventional $O(2,2)$ FDM scheme (abbreviated CONV2), and an optimally accurate $O(2,2)$ FDM predictor-corrector scheme (abbreviated OPT2);

(b) *Fourth order in space and second order in time FDM*: a conventional $O(2,4)$ FDM scheme (abbreviated CONV4), and an optimally accurate $O(2,4)$ FDM predictor-corrector scheme (abbreviated OPT4);

(c) *An SEM spatial scheme using one of the three following temporal schemes* (see Mizutani *et al*. 2000 for details): a 4th order Runge-Kutta (optimally accurate) scheme (abbreviated SEM-RK4), 2nd order conventional FDM (abbreviated SEM-CONV), and a 2nd order optimally accurate FDM scheme (abbreviated SEM-OPT).

We use the four 1-D models shown in Fig. 1 in our computational examples: a homogeneous model with periodic boundary conditions (Model A), a homogeneous model with free surface boundary conditions (Model B), a smoothly varying heterogeneous model with free surface boundary conditions (Model C), and a model with three homogeneous layers separated by sharp discontinuities, with free surface boundary conditions (Model D). The leftmost and rightmost layers of Model D, which have identical properties, remain fixed in all calculations, while the middle layer has a variable velocity v. The material properties of the models are shown in Table 1.

The following details are common to all calculations. The length of the computational domain is 3 km, and the source is a single point force with a Ricker wavelet whose central frequency is 30 Hz. The source is at the center of the model (x = 1.5 km) and is always exactly at a grid point. The duration of all calculated waveforms is 11.5 s.

In this paper the measure of the cost of the various schemes is CPU time, and the measure of accuracy (with one exception, noted below) is the relative error of the solution at the final time step, averaged over the spatial grid, defined as follows:

$$\text{r.m.s. relative error} = 100 \times \left(\frac{\sum_{i=1}^{N} (u_i^j - [u^{(0)}]_i^j)^2}{\sum_{i=1}^{N} ([u^{(0)}]_i^j)^2} \right)^{1/2}, \tag{49}$$

where N is the number of nodes, u_i^j is the calculated displacement at the ith node at the jth time step, and $[u^{(0)}]_i^j$ is the reference displacement at the ith node at the jth time step. For the homogeneous models (A and B), the exact (analytic) solution is used as the reference displacement, while

for the heterogeneous models (C and D), a numerical solution obtained with a fine spatial grid and a small time step is used. Because data from all grid points are included in the r.m.s. relative error (eq. 49), a robust measure of accuracy is obtained. The use of eq. (49) leaves open the possibility that the error at the free surface or at internal lithological discontinuities might be significantly worse than the r.m.s. error, but we show below that this is not the case.

We present results (Figs. 2–5, for models A through D respectively) showing the relation between CPU time and r.m.s. relative error for the various schemes. Each of these figures has four panels. Panel (a) shows results for the second order (in space) FDM schemes, panel (b) shows results for the fourth order (in space) FDM schemes, and panel (c) shows results for the SEM spatial schemes. The best performing scheme in each panel of Figs. 2–5 is that whose curve is closest to the lower left hand corner of the panel. Such schemes require the least CPU time to attain a given accuracy, and minimize the relative r.m.s. error for a given expenditure of CPU time.

The fourth panel (d) of each of Figs. 2–5 shows the scheme with the best performance in each of panels (a) through (c) of that figure. In cases where the choice of the best performing scheme varies with grid size, we choose the scheme with the best performance in the r.m.s. relative error range between 0.1 per cent and 1 per cent. The curves for CONV2 and CONV4 are also shown in panel (d) of Figs. 2–5 for comparison.

Each panel of Figs. 2–5 presents data for several values of the Courant number C, which we define for heterogeneous media as

$$C = \frac{\beta_{max}\Delta t}{\Delta x}, \tag{50}$$

where Δx is the spatial grid interval, Δt is the time step, and β_{max} is the maximum velocity for the model. In evaluating eq. (50) for the SEM calculations we define Δx as follows:

$$\Delta x = \frac{L_e}{N_e - 1}, \tag{51}$$

where L_e is the length of an element and N_e is the number of node points in an element. Following Komatitsch & Tromp (1999), we use $N_e = 9$ for all of the SEM calculations in this paper. We have not determined the stability criterion for the SEM schemes analytically, but empirical tests suggest that for Model A the Courant numbers for the SEM-CONV, SEM-OPT, and SEM-RK4 schemes

are respectively about 0.344, 0.596 and 0.487. In the FDM panels (a and b) of Figs. 2–5 we present computations for $C = 0.1$, 0.3, 0.5, and 0.8. In the SEM panels (c), we present computations for $C = 0.1$ and 0.3 for all SEM schemes and we also present computations for $C = 0.5$ for SEM-OPT. Each curve in panels (a) through (d) of Figs. 2–5 is plotted for a constant Courant number. We now examine the results for each model.

Fig. 2 shows results for Model A, which, as shown by Fig. 1 and Table 1, is homogeneous with periodic boundary conditions. Thus the results in all of the panels in Fig. 2 reflect the performance of the respective numerical schemes at interior points only, without effects due to external or internal boundaries or gradients in lithological properties. Fig. 2 thus provides a baseline that allows the effects of operator errors at boundaries and gradients in material properties to be studied by comparing results for Models B–D (Figs. 3–5) to those for Model A.

Fig. 2a shows that the CPU time advantage of OPT2 over CONV2 exceeds one order of magnitude in all cases, which confirms the conclusions of GT98 (except that, as the details of the respective computational experiments differ, the numerical values of the CPU time ratios are somewhat different). Note however, that for a homogeneous medium as $C \rightarrow 1$ the performance of CONV2 will approach that of OPT2 (see GT98).

Fig. 2b shows an interesting phenomenon governing the choice of the best OPT4 scheme. When the grid is relatively coarse the $O(\Delta x^4)$ error is dominant, so the best use of CPU time is to make Δx as small as possible. Thus the $C = 0.8$ scheme has the best performance, On the other hand, as Δx decreases, the $O(\Delta x^4)$ error becomes negligible compared to the $O(\Delta t^2)$ error, and the most profitable use of CPU time is to decrease the time step while keeping Δx relatively coarse; thus the $C = 0.1$ curve becomes best. However, the results in Fig. 2b show that OPT4 has a clear advantage in cost-performance over CONV4 in all cases.

Fig. 2c shows that both optimally accurate SEM schemes (SEM-OPT and SEM-RK4) far outperform an SEM scheme with non-optimally accurate time-stepping (SEM-CON). The same crossover behavior as in Fig. 2b is seen: when Δx is large the $C = 0.5$ SEM-OPT scheme is best, but as the spatial error becomes relatively negligible the $C = 0.1$ SEM-OPT scheme is best.

Fig. 2d shows the best performing (in the error range from 1 per cent to 0.1 per cent) schemes

from each of Figs. 2a–c, and, for comparison, the best performing CONV2 and CONV4 schemes. All of the optimally accurate schemes substantially outperform CONV2 and CONV4. For the ranges of likely practical interest (relative errors of 1 per cent through 0.1 per cent) OPT2 and OPT4 are superior to SEM-OPT, but for extremely small errors (5 digit accuracy, or better) SEM-OPT is best. On the basis of Fig. 2d (and as confirmed by the results presented below) it is clear that optimally accurate schemes far outperform non-optimally accurate (conventional) schemes.

Fig. 3 shows results for Model B, which is the same as Model A except that the boundary condition at both ends of the medium is a free surface rather than a periodic boundary condition. Thus any differences between Fig. 2 and Fig. 3 should be due solely to the effect of the change in boundary conditions. We see that the main difference between these two figures is the degradation in the performance of OPT4. This degradation is expected, as the result of having only three points in the first row of eq. (29) and only four points in the second row. Unlike Fig. 2d, where OPT4 was clearly (although not overwhelmingly) superior to OPT2, Fig. 3d shows that the performance of OPT2 and OPT4 is nearly equivalent (with the latter having a very slight advantage) in the range of practical interest. It is also notable that the marked “crossover” effect that was seen in Fig. 2b is almost completely absent in Fig. 3b, because of the boundary errors.

Fig. 4 shows results for a model with free surface boundary conditions, and a smooth but continuous variation in velocity. OPT4 is clearly superior to OPT2 for this case. Since, as seen in Fig. 3, the effect of the free surface boundary error was to drag OPT4 down to the level of OPT2, the re-established advantage of OPT4 evidently comes from its superiority in handling the gradients in seismic velocity. Note that in each of Fig. 2d–Fig. 4d the point at which SEM-OPT becomes most cost-effective is for relative errors smaller than 0.01 per cent.

Seismological modeling algorithms must be able to handle not only smoothly varying velocity models, but also sharp discontinuities in lithological properties. Fig. 5 shows results for such a model (Model D). The comparison of the best performing methods (Fig. 5d) shows that the curves for OPT2, OPT4 and SEM-CON all have essentially equivalent performance for a relative error of about 1 per cent. For larger errors OPT4 is best, and for smaller errors SEM-OPT is best. In all ranges OPT2 is second best. The contrast between Fig. 4 and Fig. 5 demonstrates that boundary

errors due to sharp lithological discontinuities are likely to be the factor governing the choice between numerical methods.

Figs. 2d-5d show that the performance of CONV2 is worse than CONV4 by a significant margin, but CONV4 in turn is worse by a significant margin than all of the optimally accurate methods. The results in this paper are all for 1-D examples; based on the results of Takeuchi & Geller (2000) the inferiority of CONV2 and CONV4 as compared to optimally accurate methods will be even more dramatic for 2-D and 3-D. Thus the question that numerical modelers of seismic wave propagation should be addressing is the choice among the various optimally accurate methods, rather than the choice between optimally accurate and conventional methods.

Two issues remain to be considered. The first is the question of whether boundary errors in the operators will lead to solution errors at the boundaries (at both external boundaries and internal lithological discontinuities) which are worse than at normal interior points. The answer to this question is known to be "no," based on the formal analysis of error in the frequency domain in Section 2 of GT95. There always will be a dominant mode whenever the solution is large, and the exact solution, numerical solution and the error of the numerical solution will all be (approximately) proportional to that mode. Thus the error at boundary nodes will not be significantly worse than that at interior nodes. This has been confirmed by a numerical experiment for OPT2 (Fig. 8 of GT95). We now conduct a further numerical experiment for OPT4, using Models B and D as our test cases. Fig. 6 confirms that for both models the errors at the boundaries and nodes adjacent to them are of the same order as those at typical interior points. The error shown in Fig. 6 is the error at the *i*th grid point averaged over all time steps, defined as follows:

$$(\text{point relative error})_i = 100 \times \left(\frac{\sum_{j=1}^{M} (u_i^j - [u^{(0)}]_i^j)^2}{\sum_{j=1}^{M} ([u^{(0)}]_i^j)^2} \right)^{1/2}, \tag{52}$$

where M is the number of time steps.

Finally, we study the dependence of the solution error on the amount of the velocity jump in Model D, by varying the velocity v in the middle layer. The results for OPT2 and OPT4 are shown respectively in panels a and b of Fig. 7. Note that it is clear from the form of eqs. (13) and (23) that if the velocities in Model D are equal in all layers (i.e., if $v = 2$ km/s) there will still be a boundary

error at internal boundaries if we artificially break up what is really a homogeneous layer into several different layers with overlapped mass and stiffness matrices. Fig. 7 shows the results for the single homogeneous layer as "(C)," and for the model with an artificial internal boundary as "(IB)." The latter has a notably worse error than the former for OPT4. It also is notable that as the velocity contrast between layers increases (i.e., as v decreases), the solution error degrades, particularly for OPT4.

4 DISCUSSION

The computational examples in this paper are all for 1-D models, but obviously the motivation for numerical modeling of seismic wave propagation is to make calculations for realistic 3-D (or sometimes 2-D) models. Let us now consider the implications of the results of this paper for such modeling. As discussed in the previous section, it seems clear that an optimally accurate scheme should be used. However, one major issue is the handling of lithological discontinuities. SEM can accurately handle lithological discontinuities if they coincide with the boundaries of elements. However, this means that the elements for realistic models will have complicated and irregular geometry, which will necessitate computationally intensive grid generation and memory management. Furthermore, if there are many small regions whose boundaries are first order discontinuities, it will probably be necessary to use a very small time step to ensure stability. On the other hand, optimally accurate FDM schemes of the type outlined in GT98, Takeuchi & Geller (2000) and this paper require a regularly spaced grid; if sharp lithological discontinuities fall between nodes (as will usually be the case for realistic models with arbitrarily located boundaries) much of the advantage of using optimally accurate FDM operators will be lost unless special countermeasures are taken. One promising approach to resolving this issue is that of Mizutani (2001), who developed an optimally accurate $O(2,2)$ FDM operator for cells with inter-node lithological discontinuities, while using a standard OPT2 scheme in the rest of the medium. This approach yielded excellent accuracy and may well be the best practical solution, although further work is needed to confirm this.

ACKNOWLEDGMENTS

This research was partly supported by grants from the Japan Society for the Promotion of Science (Nos. 17037001 and 17540392).

REFERENCES

Cohen, G., 2002. *High-order Numerical Method for Transient Wave Equations*, Springer.

Cohen, G. & Joly, P., 1996. Construction and analysis of fourth-order finite difference schemes for the acoustic wave equation in nonhomogeneous media, *SIAM J. num. Anal.*, **33**, 1266-1302.

Geller, R. J. & Ohminato, T., 1994. Computation of synthetic seismograms and their partial derivatives for heterogeneous media with arbitrary natural boundary conditions using the Direct Solution Method. *Geophys. J. Int.*, **116**, 421-446.

Geller, R. J. & Takeuchi, N., 1995. A new method for computing highly accurate DSM synthetic seismograms, *Geophys. J. Int.* **123**, 449-470.

Geller, R. J. & Takeuchi, N., 1998. Optimally accurate time domain second-order finite difference scheme for the elastic motion: 1-D case, *Geophys. J. Int.*, **135**, 48-62.

Geller, R. J., Hirabayashi, N. & Mizutani, H., 2005a. A comparison of staggered-grid, conventional one-step, and optimally accurate finite-difference schemes for computing synthetic seismograms, *Geophysics*, submitted.

Geller, R. J., Mizutani, H. & Hirabayashi, N., 2005b. Existence of a second range of stability of optimally accurate finite-difference schemes for numerically solving the wave equation, *SIAM J. num. Anal.*, submitted.

Komatitisch, D. & Tromp, J., 1999. Introduction to the spectral element method for three-dimensional seismic wave propagation, *Geophys. J. Int.*, **139**, 806-822.

Komatitisch, D. & Violotte, J., 1998. The spectral element method: An efficient tool to simulate the seismic response of 2D and 3D geological structures, *Bull. seism. Soc. Amer.*, **88**, 368-392.

Levander, A. R., 1988. Fourth-order finite-difference P-SV seismograms, *Geophysics*, **53**, 1425-1436.

Mizutani, H., 2001. *Accurate and Efficient Methods for Calculating Synthetic Seismograms when Elastic Discontinuities Do not Coincide with the Numerical Grid*, D. Sc. Thesis, University of Tokyo.

Mizutani, H., Geller, R. J. & Takeuchi, N., 2000. Comparison of accuracy and efficiency of time-domain schemes for calculating synthetic seismograms, *Phys. Earth planet. Int.*, **119**, 75-97.

Robertsson, J. O. A., Blanch, J. O. & Symes, W. W., 1994. Viscoelastic finite-difference modeling, *Geophysics*, **59**, 1444-1456.

Takeuchi, N. & Geller, R. J., 2000. Optimally accurate second-order time-domain finite difference scheme for computing synthetic seismograms in 2-D and 3-D media, *Phys. Earth planet. Int.*, **119**, 103-138.

APPENDIX A: IMPLEMENTATION OF ALGORITHMS

We give the explicit form and required floating point operation counts for the conventional and modified operators for the general inhomogeneous problem at an interior point. For simplicity, we consider homogeneous temporal and spatial grid intervals Δt and Δx. A first order discontinuity in elastic properties or spatial grid interval can be handled by overlapping (see Fig. 3 of GT95). The modification of the following scheme to the case of boundary nodes or nodes immediately adjacent to boundary nodes is straightforward, but we do not present the explicit form of the scheme.

A1 Predictor Step

The 1-D conventional scheme is used as the predictor step (see eqs. 8-10). The explicit scheme for the 1-D heterogeneous problem using the stencils for the conventional operators (eqs. 3 and 29) is as follows:

$$\begin{aligned} c_n^{N+1} \;=\; & -c_n^{N-1} \\ & -\left(\frac{\mu_{n-2}+\mu_n}{24\rho_n}\,\frac{\Delta t^2}{\Delta x^2}\right) c_{n-2}^N \\ & +\left(\frac{16(\mu_{n-1}+\mu_n)}{24\rho_n}\,\frac{\Delta t^2}{\Delta x^2}\right) c_{n-1}^N \\ & +\left(2-\left(\frac{16(\mu_{n-1}+2\mu_n+\mu_{n+1})-(\mu_{n-2}+2\mu_n+\mu_{n+2})}{24\rho_n}\right)\,\frac{\Delta t^2}{\Delta x^2}\right) c_n^N \\ & +\left(\frac{16(\mu_n+\mu_{n+1})}{24\rho_n}\,\frac{\Delta t^2}{\Delta x^2}\right) c_{n+1}^N \\ & -\left(\frac{\mu_n+\mu_{n+2}}{24\rho_n}\,\frac{\Delta t^2}{\Delta x^2}\right) c_{n+2}^N \\ & +\left(\frac{\Delta t^2}{\rho_n} F_n^N\right), \end{aligned} \tag{A1}$$

where c_n^N and F_n^N are the displacement and the body force at x and t respectively, and ρ_n and μ_n are the density and rigidity at x respectively. c_n^{N+1} is the unknown displacement at $t+\Delta t$ to be determined; the other quantities in eq. (A1) are all known.

Note that in this Appendix we write c_n^N to denote the displacement computed by the predictor step, whereas we used c^0 in eq. (8). The coefficients in parentheses in eq. (A1) can be computed once for each node n and stored. Because the body force term F_n^N will be zero except for a small

number number of space-time points, we ignore it in the remainder of this section. Ignoring the body force term, the floating operation counts required for the predictor step are as follows for computing the new displacement at one node for one time step:

$$\boxed{\text{5 MULS, 5 ADDS}}\,.$$

A2 Corrector Step

The optimally accurate temporal operator for the predictor step is given by eq. (6), except that the density ρ must be replaced by ρ_n, the density at each node point. The optimally accurate spatial operator for the predictor step is obtained from eq. (24) in the same way that eq. (7) is obtained from eq. (4), although its explicit form is not given in the body of the paper. Using the fact that $\delta c_n^N = \delta c_n^{N-1} = 0$, the explicit discretized equation for the correction step (eq. 9) is as follows :

$$\begin{aligned}
\delta c_n^{N+1} \;=\; & \left(\frac{1}{90} - \frac{\mu_{n-2}+\mu_n}{288\rho_n}\,\frac{\Delta t^2}{\Delta x^2}\right)\left[c_{n-2}^{N+1} - 2c_{n-2}^{N} + c_{n-2}^{N-1}\right] \\
& + \left(-\frac{4}{90} + \frac{16(\mu_{n-1}+\mu_n)}{288\rho_n}\,\frac{\Delta t^2}{\Delta x^2}\right)\left[c_{n-1}^{N+1} - 2c_{n-1}^{N} + c_{n-1}^{N-1}\right] \\
& + \left(\frac{6}{90} - \frac{16(\mu_{n-1}+2\mu_n+\mu_{n+1}) - (\mu_{n-2}+2\mu_n+\mu_{n+2})}{288\rho_n}\,\frac{\Delta t^2}{\Delta x^2}\right)\left[c_{n}^{N+1} - 2c_{n}^{N} + c_{n}^{N-1}\right] \\
& + \left(-\frac{4}{90} + \frac{16(\mu_{n}+\mu_{n+1})}{288\rho_n}\,\frac{\Delta t^2}{\Delta x^2}\right)\left[c_{n+1}^{N+1} - 2c_{n+1}^{N} + c_{n+1}^{N-1}\right] \\
& + \left(\frac{1}{90} - \frac{\mu_{n}+\mu_{n+2}}{288\rho_n}\,\frac{\Delta t^2}{\Delta x^2}\right)\left[c_{n+2}^{N+1} - 2c_{n+2}^{N} + c_{n+2}^{N-1}\right] \qquad \text{(A2)}
\end{aligned}$$

The coefficients in parentheses in eq. (A2) can be computed once for each node and stored. Furthermore, the first four bracketed terms in eq. (A2) will have been previously computed for the loops for adjacent nodes and can be reused. Thus only the last bracketed term need be computed at this point. As $2c_{n+2}^N$ can be computed by addition of $(c_{n+2}^N + c_{n+2}^N)$, we count this as an addition operation, rather than a multiplication. Thus the operation count for the corrector step is 5 multiplications and 7 additions.

Finally, after computing δc_n^{N+1} for all nodes, and before proceeding to the next time step, we combine eqs. (A2) and (A1) to get the net corrected displacement:

$$c_n^{N+1} \leftarrow c_n^{N+1} + \delta c_n^{N+1}, \qquad \text{(A3)}$$

where we use $\leftarrow$ to denote a replacement rather than a mathematical equality.

Combining the 5 multiplications and 5 additions for the predictor scheme (eq. A1), 5 multiplications and 7 additions for the corrector scheme (eq. A2), and 1 addition for the update (eq. A3), the total operation count is as follows:

$$\boxed{\text{10 MULS, 13 ADDS}}\,.$$

Thus the operation count for the optimally accurate (predictor-corrector) $O(2,4)$ scheme is about double that of the conventional (predictor only) $O(2,4)$ scheme.

APPENDIX B: STABILITY CONDITIONS AND NUMERICAL DISPERSION OF FD SCHEMES

B1 Stability of O$(2,4)$ predictor-corrector scheme

We begin by determining the maximum time step (Courant number) for the $O(2,4)$ predictor-corrector scheme (eqs. 8-10). We consider only the case of an infinite homogeneous medium, but based on the results of GT98 and Takeuchi & Geller (2000) for $O(2,2)$ schemes, the results obtained in this section can be applied approximately to a heterogeneous medium with free boundaries by using, say, 95 per cent of the smallest value of the "local Δt" as the time step.

We show below that the stability limit for the implicit $O(2,4)$ scheme has a small but non-negligible difference with the stability limit for the $O(2,4)$ predictor-corrector scheme. In contrast, as also shown below, this is not the case for the respective $O(2,2)$ schemes, for which the stability limits are equal.

We begin by considering the $O(2,4)$ predictor-corrector scheme. The difference stencils for the predictor step are given by eqs. (3) and (4). We write the predictor step as follows:

$$\tilde{c}_n^{N+1} - 2c_n^N + c_n^{N-1} = \mathcal{C}^2 \mathbf{L}^{(2)} \mathbf{c}_n^N, \tag{B1}$$

where c_n^N and c_n^{N-1} are the corrected values of the displacement at the nth node at the present (Nth) and past ($N-1$th) time steps, and $\tilde{c}_n^{N+1}$ is the uncorrected value of the displacement at the nth node at the future ($N+1$th) time step, to be found by the predictor step, and where

$$C^2 = \frac{\beta^2 \Delta t^2}{\Delta x^2}, \tag{B2}$$

where

$$\beta = \sqrt{\frac{\mu}{\rho}} \tag{B3}$$

is the velocity of wave propagation.

The operator on the r.h.s. of eq. (B1) is defined as follows:

$$\mathbf{L}^{(2)} = \begin{pmatrix} L_{-2}^{(2)} & L_{-1}^{(2)} & L_0^{(2)} & L_1^{(2)} & L_2^{(2)} \end{pmatrix} = \frac{1}{12}\begin{pmatrix} -1 & 16 & -30 & 16 & -1 \end{pmatrix}, \tag{B4}$$

and the operation of $\mathbf{L}^{(2)}$ on a vector is defined as follows:

$$\mathbf{L}^{(2)}\mathbf{c}_n^N = \sum_{j=-2}^{2} L_j^{(2)} c_{n+j}^N \tag{B5}$$

We also define the following operator which is used in the corrector step:

$$\mathbf{L}^{(4)} = \begin{pmatrix} L_{-2}^{(4)} & L_{-1}^{(4)} & L_0^{(4)} & L_1^{(4)} & L_2^{(4)} \end{pmatrix} = \frac{1}{90}\begin{pmatrix} -1 & 4 & -6 & 4 & -1 \end{pmatrix}; \tag{B6}$$

the operation of $\mathbf{L}^{(4)}$ on a vector is defined as follows:

$$\mathbf{L}^{(4)}\mathbf{c}_n^N = \sum_{j=-2}^{2} L_j^{(4)} c_{n+j}^N. \tag{B7}$$

Using the above definitions, we now evaluate the correction term (given by eq. 9, using the operators in eqs 11 and 12, and the stencils in eqs. 3–7) as follows:

$$\begin{aligned} \delta c_n^{N+1} &= -\left(\mathbf{L}^{(4)}\tilde{\mathbf{c}}_n^{N+1} - 2\mathbf{L}^{(4)}\mathbf{c}_n^N + \mathbf{L}^{(4)}\mathbf{c}_n^{N-1}\right) \\ &\quad + \frac{C^2}{12}\left(\mathbf{L}^{(2)}\tilde{\mathbf{c}}_n^{N+1} - 2\mathbf{L}^{(2)}\mathbf{c}_n^N + \mathbf{L}^{(2)}\mathbf{c}_n^{N-1}\right) \\ &= -\mathbf{L}^{(4)}\left(\tilde{\mathbf{c}}_n^{N+1} - 2\mathbf{c}_n^N + \mathbf{c}_n^{N-1}\right) \\ &\quad + \frac{C^2}{12}\mathbf{L}^{(2)}\left(\tilde{\mathbf{c}}_n^{N+1} - 2\mathbf{c}_n^N + \mathbf{c}_n^{N-1}\right) \\ &= -C^2\mathbf{L}^{(4)}\mathbf{L}^{(2)}\mathbf{c}_n^N + \frac{C^4}{12}\mathbf{L}^{(2)}\mathbf{L}^{(2)}\mathbf{c}_n^N, \end{aligned} \tag{B8}$$

where we used eq. (B1) to obtain the last line of eq. (B8). Note that

$$\mathbf{L}^{(2)}\mathbf{L}^{(2)}\mathbf{c}_n^N = \mathbf{L}^{(2,2)}\mathbf{c}_n^N = \sum_{j=-2}^{2}\sum_{k=-2}^{2} L_j^{(2)} L_k^{(2)} c_{n+j+k}^N \tag{B9}$$

$$\mathbf{L}^{(4)}\mathbf{L}^{(2)}\mathbf{c}_n^N = \mathbf{L}^{(4,2)}\mathbf{c}_n^N = \sum_{j=-2}^{2}\sum_{k=-2}^{2} L_j^{(4)} L_k^{(2)} c_{n+j+k}^N \tag{B10}$$

The operators on the r.h.s. of eqs. (B9)–(B10) are defined as follows:

$$\mathbf{L}^{(2,2)} = \begin{pmatrix} L_{-4}^{(2,2)} & L_{-3}^{(2,2)} & L_{-2}^{(2,2)} & L_{-1}^{(2,2)} & L_{0}^{(2,2)} & L_{1}^{(2,2)} & L_{2}^{(2,2)} & L_{3}^{(2,2)} & L_{4}^{(2,2)} \end{pmatrix}$$
$$\frac{1}{144}\begin{pmatrix} 1 & -32 & 316 & -992 & 1414 & -992 & 316 & -32 & 1 \end{pmatrix} \quad \text{(B11)}$$

$$\mathbf{L}^{(4,2)} = \begin{pmatrix} L_{-4}^{(4,2)} & L_{-3}^{(4,2)} & L_{-2}^{(4,2)} & L_{-1}^{(4,2)} & L_{0}^{(4,2)} & L_{1}^{(4,2)} & L_{2}^{(4,2)} & L_{3}^{(4,2)} & L_{4}^{(4,2)} \end{pmatrix}$$
$$\frac{1}{1080}\begin{pmatrix} 1 & -20 & 100 & -236 & 310 & -236 & 100 & -20 & 1 \end{pmatrix} \quad \text{(B12)}$$

We now sum the l.h.s. and r.h.s. of eqs. (B1) and (B8) to obtain the following one-step scheme which is rigorously equal to the predictor-corrector scheme.

$$c_n^{N+1} - 2c_n^N + c_n^{N-1} = C^2\mathbf{L}^{(2)}\mathbf{c}_n^N - C^2\mathbf{L}^{(4,2)}\mathbf{c}_n^N + \frac{C^4}{12}\mathbf{L}^{(2,2)}\mathbf{c}_n^N. \quad \text{(B13)}$$

Note that the future term on the l.h.s. of eq. (B1) is $\tilde{c}_n^{N+1}$ but the corresponding term in eq. (B13) is c_n^{N+1}, because the predictor and corrector have been summed. Also note that the steps we followed to obtain eq. (B13) are essentially the same as those followed to show that predictor-corrector schemes and Lax-Wendroff schemes are equivalent (Mizutani *et al*. 2000).

In order to determine the stability limit we substitute a harmonic solution of the form

$$c_{n+m}^{N+l} = \exp(\mathrm{i}l\omega\Delta t)\exp(\mathrm{i}mk\Delta x), \quad \text{(B14)}$$

where $\mathrm{i} = \sqrt{-1}$, m and l are spatial and temporal indices respectively, ω is the frequency, and k is the wavenumber, into eq. (B13). Using eqs. (B6), (B7), and (B9)–(B12), we obtain

$$\begin{aligned}(2A-2) &= \frac{C^2}{12}(-30+32E-2F) \\ &\quad -\frac{C^2}{1080}(310-472E+200F-40G+2H) \\ &\quad +\frac{C^4}{1728}(1414-1984E+632F-64G+2H), \end{aligned} \quad \text{(B15)}$$

where

$$\begin{aligned} A &= \cos(\omega\Delta t) \\ E &= \cos(k\Delta x) \\ F &= \cos(2k\Delta x) = 2E^2 - 1 \\ G &= \cos(3k\Delta x) = 4E^3 - 3E \end{aligned}$$

$$H \;=\; \cos(4k\Delta x) = 8E^4 - 8E^2 + 1 \tag{B16}$$

The well known conditions for stability are that A should be real and that $1 \geq A \geq -1$. The maximum value of A occurs when $E = F = G = H = 1$; we see from eq. (B15) that $A = 1$ for this case. The minimum value of A occurs when $E = -F = G = -H = -1$. For this case we have, from eq. (B15),

$$A = 1 - \frac{424}{135}C^2 + \frac{32}{27}C^4 \geq -1, \tag{B17}$$

from which we obtain the inequality,

$$1 - \frac{212}{135}C^2 + \frac{16}{27}C^4 \geq 0. \tag{B18}$$

Eq. (B18) is satisfied when

$$C^2 \leq \frac{53 - \sqrt{109}}{40} \approx 1.06399, \tag{B19}$$

which means that the stability condition for the optimally accurate $O(2,4)$ predictor-corrector scheme is approximately

$$C < 1.0315. \tag{B20}$$

It is interesting that this is a slightly larger value than Courant's famous result for the conventional $O(2,2)$ scheme.

Note that $-1 \leq A \leq 1$ is also satisfied when

$$(53 + \sqrt{109})/40 \approx 1.5860 \leq C^2 \leq 53/20 = 2.6500, \tag{B21}$$

i.e., when

$$1.2593 \leq C \leq 1.6279. \tag{B22}$$

This is because when eqs. (B21) and (B22) are satisfied, $-1 \leq A \leq 1$ is satisfied not only for $E = -1$ but for all $-1 \leq E \leq 1$ (Geller *et al.* 2005b). The above second window of stability may not necessarily be of practical importance, because the range for which Δt is stable would vary with position in a heterogeneous medium, and it might thus be difficult to ensure stability everywhere. It is, however, an interesting phenomenon that has not, to our knowledge, been previously reported. We have verified by a numerical experiment for a medium with periodic boundary conditions that

this second range is indeed stable, while values slightly outside the range in eqs. (B21) or (B22) are unstable.

B2 Stability of O$(2,4)$ implicit scheme

In practice, only the predictor-corrector realization of the $O(2,4)$ scheme is likely to be used, but for completeness we also determine the maximum time step for the $O(2,4)$ implicit scheme (eq. 2, using the stencils eqs. 6–7). We substitute a solution of the form eq. (B14) into eq. (2) and, using eq. (B16), we obtain the dispersion relation:

$$\frac{1}{90}(84+8E-2F)(2A-2)=\frac{C^2}{144}(-30+32E-2F)(10+2A). \tag{B23}$$

We solve eq. (B23) for A, obtaining:

$$A=\frac{C^2(-375+400E-25F)+(336+32E-8F)}{C^2(75-80E+5F)+(336+32E-8F)} \tag{B24}$$

The condition for stability is $-1\le A\le 1$. As $A=1$ when $E=F=1$, $A\le 1$ is satisfied. The condition $-1\le A$ is hardest to satisfy when $E=-F=-1$. For that case we obtain, from eq. (B24),

$$A=\frac{-100C^2+37}{20C^2+37}>-1, \tag{B25}$$

which is satisfied when

$$C^2<\frac{37}{40}. \tag{B26}$$

B3 Stability of O$(2,2)$ predictor-corrector scheme

We follow basically the same steps used above for the $O(2,4)$ predictor-corrector scheme to determine the stability limit for the $O(2,2)$ optimally accurate predictor-corrector scheme. The conventional FD operators $\mathbf{A^0}$ and $\mathbf{K^0}$, and the optimally accurate FD operators $\mathbf{A}$ and $\mathbf{K}$ are as follows (see GT98 for details):

$$\mathbf{A^0} = \left(\frac{\rho}{\Delta t^2}\right) \times$$

	$x-\Delta x$	x	$x+\Delta x$
$t+\Delta t$		1	
t		-2	
$t-\Delta t$		1	

$$\mathbf{K^0} = \left(\frac{\mu}{\Delta x^2}\right) \times$$

	$x-\Delta x$	x	$x+\Delta x$
$t+\Delta t$			
t	1	-2	1
$t-\Delta t$			

(B27)

$$\mathbf{A} = \left(\frac{\rho}{\Delta t^2}\right) \times$$

	$x-\Delta x$	x	$x+\Delta x$
$t+\Delta t$	$1/12$	$10/12$	$1/12$
t	$-2/12$	$-20/12$	$-2/12$
$t-\Delta t$	$1/12$	$10/12$	$1/12$

(B28)

$$\mathbf{K} = \left(\frac{\mu}{\Delta x^2}\right) \times$$

	$x-\Delta x$	x	$x+\Delta x$
$t+\Delta t$	$1/12$	$-2/12$	$1/12$
t	$10/12$	$-20/12$	$10/12$
$t-\Delta t$	$1/12$	$-2/12$	$1/12$

.

Eqs. (B1), (B2), (B8), and (B13), derived above for the $O(2,4)$ scheme, hold without change for the $O(2,2)$ scheme. The operators in eqs. (B4), (B6), (B11), and (B12) are redefined as follows:

$$\mathbf{L}^{(2)} = \begin{pmatrix} L_{-1}^{(2)} & L_0^{(2)} & L_1^{(2)} \end{pmatrix} = \begin{pmatrix} 1 & -2 & 1 \end{pmatrix} \tag{B29}$$

$$\mathbf{L}^{(4)} = \frac{1}{12}\mathbf{L}^{(2)} \tag{B30}$$

$$\mathbf{L}^{(2,2)} = \begin{pmatrix} L_{-2}^{(2,2)} & L_{-1}^{(2,2)} & L_0^{(2,2)} & L_1^{(2,2)} & L_2^{(2,2)} \end{pmatrix} = \begin{pmatrix} 1 & -4 & 6 & -4 & 1 \end{pmatrix} \tag{B31}$$

$$\mathbf{L}^{(4,2)} = \frac{1}{12}\mathbf{L}^{(2,2)} \tag{B32}$$

In accordance with the above definitions, eqs. (B5), (B7), (B9), and (B10) are modified, so that the limits of summation are -1 to 1 rather than -2 to 2.

Using the above definitions and modifications, we substitute eq. (B14) into eq. (B13) to obtain the following dispersion relation (using eq. B16):

$$(2A-2) = C^2(2E-2) + (6-8E+2F)\left(\frac{C^4}{12} - \frac{C^2}{12}\right). \tag{B33}$$

When $E = F = 1$ we have $A = 1$. When $E = -F = -1$ we obtain

$$A = 1 - \frac{8}{3}C^2 + \frac{2}{3}C^4 \tag{B34}$$

For $E = -F = -1$ the stability condition $-1 \leq A \leq 1$ is satisfied for either of the following two ranges:

$$0 \quad \leq C^2 \leq 1 \tag{B35}$$

$$3 \quad \leq C^2 \leq 4, \tag{B36}$$

where eq. (B35) is the range of practical interest. Unlike the $O(2,4)$ predictor-corrector case (see above) the second stability range (eq. B36) for $E = -1$ is not stable for all possible values of E, so, in contrast to the optimally accurate $O(2,4)$ predictor-corrector scheme, the optimally accurate $O(2,2)$ predictor-corrector scheme does not have a second range of stability. For the point $C^2 = 4$ the stability condition is formally satisfied for all $-1 \leq E \leq 1$ (see Geller *et al*. 2005b), but this case does not seem to be of practical importance.

B4 Stability of O$(2,2)$ implicit scheme

In practice, only the predictor-corrector realization of the $O(2,2)$ scheme is likely to be used, but we also present the maximum time step for the $O(2,2)$ implicit scheme (eq. 2, using the stencils eqs. B28). (This result was also given by GT98, so our discussion here is brief.)

We substitute a solution of the form eq. (B14) into eq. (2) and, using eq. (B16), we obtain the dispersion relation:

$$\frac{1}{12}(10+2E)(2A-2) = \frac{C^2}{12}(2E-2)(10+2A). \tag{B37}$$

We solve eq. (B37) for A, obtaining:

$$A = \frac{5C^2(E-1) + (5+E)}{-C^2(E-1) + (5+E)} \tag{B38}$$

The condition for stability is $-1 \leq A \leq 1$. As $A = 1$ when $E = 1$, $A \leq 1$ is satisfied. The condition $-1 \leq A$ is hardest to satisfy when $E = -1$, For that case we obtain, from eq. (B38),

$$A = \frac{-5C^2+2}{C^2+2} > -1, \tag{B39}$$

which is satisfied when

$$C^2 < 1. \tag{B40}$$

B5 Numerical dispersion of phase velocity of optimally accurate schemes

Since (see eq. B16)

$$\cos^{-1} A = \omega \Delta t, \tag{B41}$$

and since the numerical phase velocity is

$$\beta_{num} = \frac{\omega}{k}, \tag{B42}$$

we have

$$\beta_{num} = \frac{\cos^{-1} A}{k\Delta t}. \tag{B43}$$

Using eq. (B43), we obtain the following expressions for the numerical dispersion of the phase velocity of the respective schemes from eqs. (B15), (B24), (B33), and (B38):

$$\begin{aligned}
\beta_{PC4} &= \frac{1}{k\Delta t}\cos^{-1}\left[1+\frac{C^2}{12}(-15+16E-F)\right. \\
&\quad -\frac{C^2}{1080}(155-236E+100F-10G+H) \\
&\quad \left.+\frac{C^4}{1728}(707-992E+316F-32G+H)\right], \\
&\approx \beta\left[1-C^4\frac{k^4\Delta x^4}{720}+\cdots\right] \qquad \text{(B44)} \\
\beta_{im4} &= \frac{1}{k\Delta t}\cos^{-1}\left[\frac{C^2(-375+400E-25F)+(336+32E-8F)}{C^2(75-80E+5F)+(336+32E-8F)}\right] \\
&\approx \beta\left[1+C^4\frac{k^4\Delta x^4}{480}+\cdots\right] \qquad \text{(B45)} \\
\beta_{PC2} &= \frac{1}{k\Delta t}\cos^{-1}\left[1+C^2(E-1)+(3-4E+F)\left(\frac{C^4}{12}-\frac{C^2}{12}\right)\right] \\
&\approx \beta\left[1-(4-5C+C^2)\frac{k^4\Delta x^4}{720}+\cdots\right] \qquad \text{(B46)}
\end{aligned}$$

$$
\begin{aligned}
\beta_{im2} &= \frac{1}{k\Delta t}\cos^{-1}\left[\frac{5C^2(E-1)+(5+E)}{-C^2(E-1)+(5+E)}\right] \\
&= \frac{1}{k\Delta t}\cos^{-1}\left[\frac{1+(E-1)(5C^2+1)/6}{1+(E-1)(-C^2+1)/6}\right] \\
&\approx \frac{1}{k\Delta t}\cos^{-1}\left[\left(1+\frac{(E-1)(5C^2+1)}{6}\right)\right. \\
&\quad \left.\left(1-\frac{(E-1)(-C^2+1)}{6}+\frac{(E-1)^2(-C^2+1)^2}{36}-\frac{(E-1)^3(-C^2+1)^3}{216}+\cdots\right)\right] \\
&\approx \frac{1}{k\Delta t}\cos^{-1}\left[1+C^2(E-1)+\frac{(C^4-C^2)(E-1)^2}{6}\right. \\
&\quad \left.+\frac{(C^6-2C^4+C^2)(E-1)^3}{36}+\cdots\right] \\
&\approx \frac{1}{k\Delta t}\cos^{-1}\left[1+C^2\left(-\frac{k^2\Delta x^2}{2}+\frac{k^4\Delta x^4}{24}-\frac{k^6\Delta x^6}{720}+\cdots\right)\right. \\
&\quad \left.+\frac{(C^4-C^2)}{6}\left(\frac{k^4\Delta x^4}{4}-\frac{k^6\Delta x^6}{24}+\cdots\right)+\frac{(C^6-2C^4+C^2)}{36}\left(-\frac{k^6\Delta x^6}{8}+\cdots\right)+\cdots\right] \\
&\approx \frac{1}{k\Delta t}\cos^{-1}\left[\left(1-\frac{C^2k^2\Delta x^2}{2}+\frac{C^4k^4\Delta x^4}{24}-\frac{C^6k^6\Delta x^6}{720}+\cdots\right)\right. \\
&\quad \left.+\left((C^2-C^6)\frac{k^6\Delta x^6}{480}+\cdots\right)\right] \qquad \text{(B47)} \\
&\approx \frac{1}{k\Delta t}\cos^{-1}\left[\cos(Ck\Delta x)+\left((C^2-C^6)\frac{k^6\Delta x^6}{480}+\cdots\right)\right] \\
&\approx \frac{1}{k\Delta t}\left[Ck\Delta x-\left(\frac{1}{\sqrt{1-\cos^2(Ck\Delta x)}}\right)(C^2-C^6)\frac{k^6\Delta x^6}{480}+\cdots\right] \\
&\approx \frac{1}{k\Delta t}\left[Ck\Delta x-\left(\frac{1}{Ck\Delta x}\right)C^2(1-C^4)\frac{k^6\Delta x^6}{480}+\cdots\right] \\
&\approx \frac{1}{k\Delta t}\left[Ck\Delta x-C(1-C^4)\frac{k^5\Delta x^5}{480}+\cdots\right] \\
&\approx \beta\left[1-(1-C^4)\frac{k^4\Delta x^4}{480}+\cdots\right] \qquad \text{(B48)}
\end{aligned}
$$

Note that we used the following approximations, assuming ε is small:

$$\cos\varepsilon = 1-\frac{\varepsilon^2}{2}+\frac{\varepsilon^4}{24}-\frac{\varepsilon^6}{720}+\cdots \qquad \text{(B49)}$$

$$\cos^{-1}(x+\varepsilon) = \cos^{-1}x-\frac{\varepsilon}{\sqrt{1-x^2}}+\cdots \qquad \text{(B50)}$$

to evaluate the lowest order term of the numerical dispersion of the phase velocity. The steps for deriving the lowest order term of the numerical dispersion are shown only for the simplest case, eq. (B48), but are basically the same for the other three cases, for which only the final result is

shown. These derivations are tedious if carried out by hand, but are straightforward if Matlab is used.

B6 Results for Conventional Schemes

For comparison we give the stability limit, dispersion equations, and low wavenumber approximation for conventional $O(2,2)$, and $O(2,4)$ schemes. As these are well known and easily derived results we omit the derivations.

The difference stencils for the conventional $O(2.2)$ scheme for a homogeneous medium are given by eq. (B27). For this scheme we have:

$$C^2 \leq 1 \tag{B51}$$

$$2A-2 = C^2(2E-2) \tag{B52}$$

$$\beta_{C2} \approx \beta\left(1-(1-C^2)\frac{k^2\Delta x^2}{24}+\cdots\right) \tag{B53}$$

The difference stencils for the conventional $O(2.4)$ scheme for a homogeneous medium are given by eq. (3) and eq. (4). For this scheme we have:

$$C^2 \leq 3/4 \tag{B54}$$

$$2A-2 = \frac{C^2}{12}(-2F+32E-30) \tag{B55}$$

$$\begin{aligned}\beta_{C4} &= \frac{1}{k\Delta t}\cos^{-1}\left[1+\frac{C^2}{12}(-15+16E-F)\right] \\ &\approx \frac{1}{k\Delta t}\cos^{-1}\left[\left(1-\frac{C^2k^2\Delta x^2}{2}+\frac{C^2k^6\Delta x^6}{180}+\cdots\right)\right] \qquad \text{(B56)} \\ &\approx \beta\left(1+C^2\frac{k^2\Delta x^2}{24}+\cdots\right) \qquad \text{(B57)}\end{aligned}$$

Note that even though the spatial operator (eq. 4) is fourth order, the numerical dispersion of the phase velocity for the conventional $O(2,4)$ scheme is second order in Δx. In contrast, as shown above, the numerical dispersion of the phase velocity for all of the optimally accurate schemes (both $O(2,4)$ and $O(2,2)$) is fourth order in Δx. As the conventional $O(2,4)$ scheme does not satisfy the criterion for optimally accurate operators of GT95, this is, in one sense, an obvious and expected result. However, for readers not familiar with the theory of GT95, it seems worthwhile

to explain the reason for the poor accuracy of the conventional $O(2,4)$ scheme using the above results directly.

Let us compare the numbered intermediate steps, eqs. (B47) and (B56), in the respective derivations of β_{im4} and β_{C4}. We can see that the term

$$\frac{C^4 k^4 \Delta x^4}{24}$$

is present in the argument of $\cos^{-1}$ in the former equation, but is absent in the latter equation. It is the absence of this term in the latter equation that is responsible for the error of the phase velocity of the conventional $O(2,4)$ scheme being $O(\Delta x^2)$ rather than $O(\Delta x^4)$. In other words, ironically, the error of the numerical dispersion of the phase velocity of the conventional $O(2,4)$ scheme is $O(\Delta x^2)$ precisely because the error of the spatial operator is $O(\Delta x^4)$. What is needed instead is for the error of the spatial operator to be tuned to match the error of the temporal operator. This is smoothly and essentially automatically achieved using the general criterion for optimally accurate operators of GT95.

However, by comparing the highest order term in eq. (B56) with the desired term above, we can see that in certain fortuitous special cases the conventional $O(2,4)$ scheme will obtain a highly accurate numerical phase velocity (and thus a solution error close to that achieved by optimal accuracy) when the following condition is satisfied:

$$\frac{C^2 k^6 \Delta x^6}{180} = \frac{C^4 k^4 \Delta x^4}{24}. \tag{B58}$$

We see that eq. (B58) will be satisfied when

$$k = \sqrt{\frac{15}{2}} \frac{C}{\Delta x} \approx 2.74 \frac{C}{\Delta x}. \tag{B59}$$

Thus CONV4 will achieve near-optimal accuracy for wavenumbers near the value in eq. (B59). The wavefield will always contain a wide spectrum of wavenumbers, but in cases where the dominant wavenumber is close to that in eq. (B59), the overall relative error will tend to be close to that of optimally accurate schemes. As the Courant number becomes smaller, the wavenumber for which fortuitous nearly optimal accuracy will be achieved by the conventional $O(2,4)$ scheme will also become smaller, which is confirmed by the results shown in Figs. 2b–5b, and also by other numerical experiments we have conducted.

Model	x	β(km/s)	ρ(kg/m^3)	B.C.
A	$0 \leq x \leq 3$	2	1000	Periodic
B	$0 \leq x \leq 3$	2	1000	Free
C	$0 \leq x \leq 3$	$1.5 + 0.5\cos(2\pi x/3)$	1000	Free
D	$0 \leq x \leq 0.75$	2	1000	Free at $x = 0$
	$0.75 \leq x \leq 2.25$	v	1000	
	$2.25 \leq x \leq 3$	2	1000	Free at $x = 3$

Table 1. Material properties of the models.

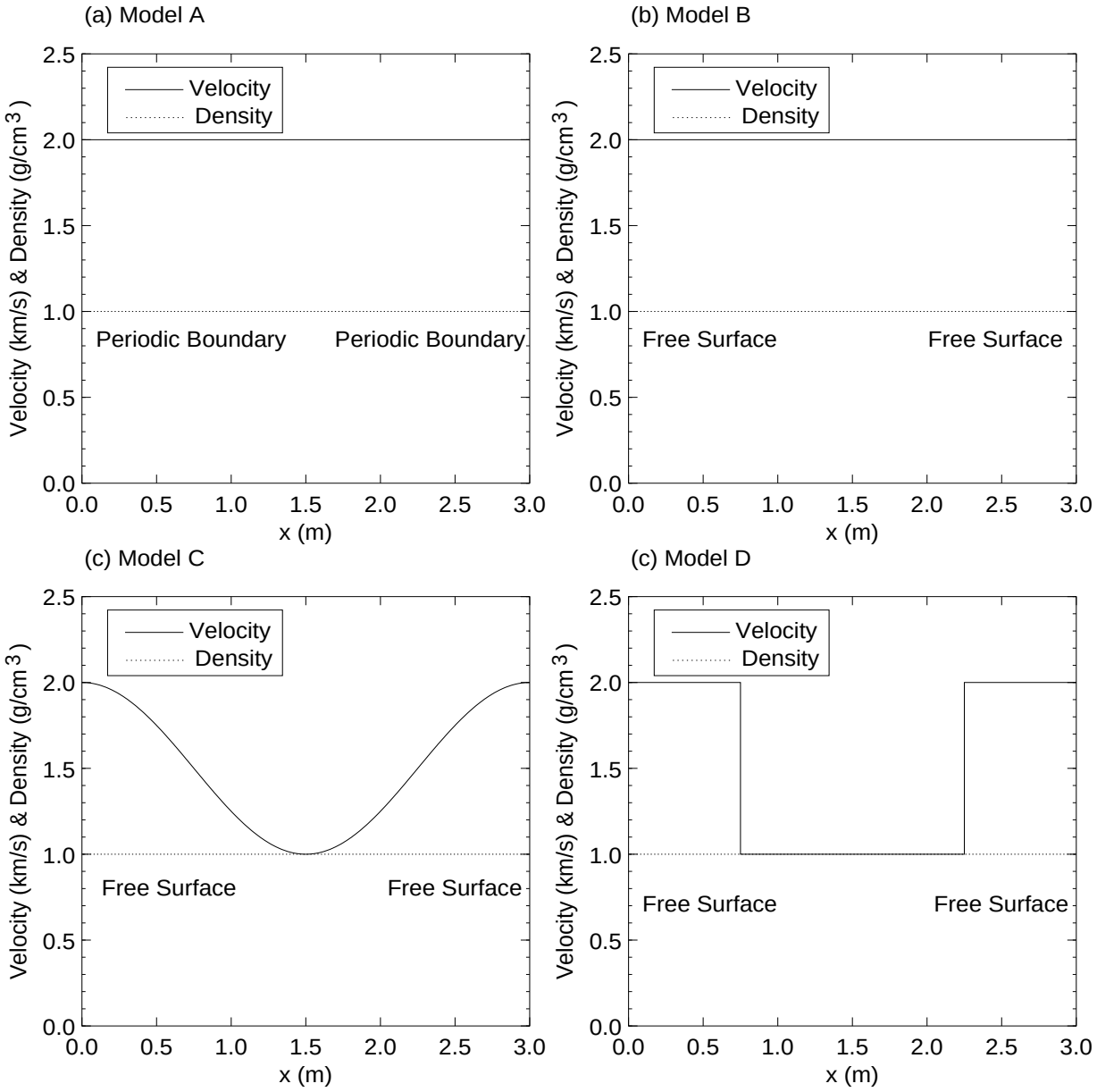

Figure 1. Models for computational examples. (a) Model A: a homogeneous layer with periodic boundary conditions (upper left), (b) Model B: a homogeneous layer with free surface boundary conditions (upper right), (c) Model C: a smoothly varying heterogeneous layer with free surface boundary conditions (lower left) and (d) Model D: discontinuous two-layered model with free surface boundary conditions (lower right). Detailed properties are shown in Table 1

.

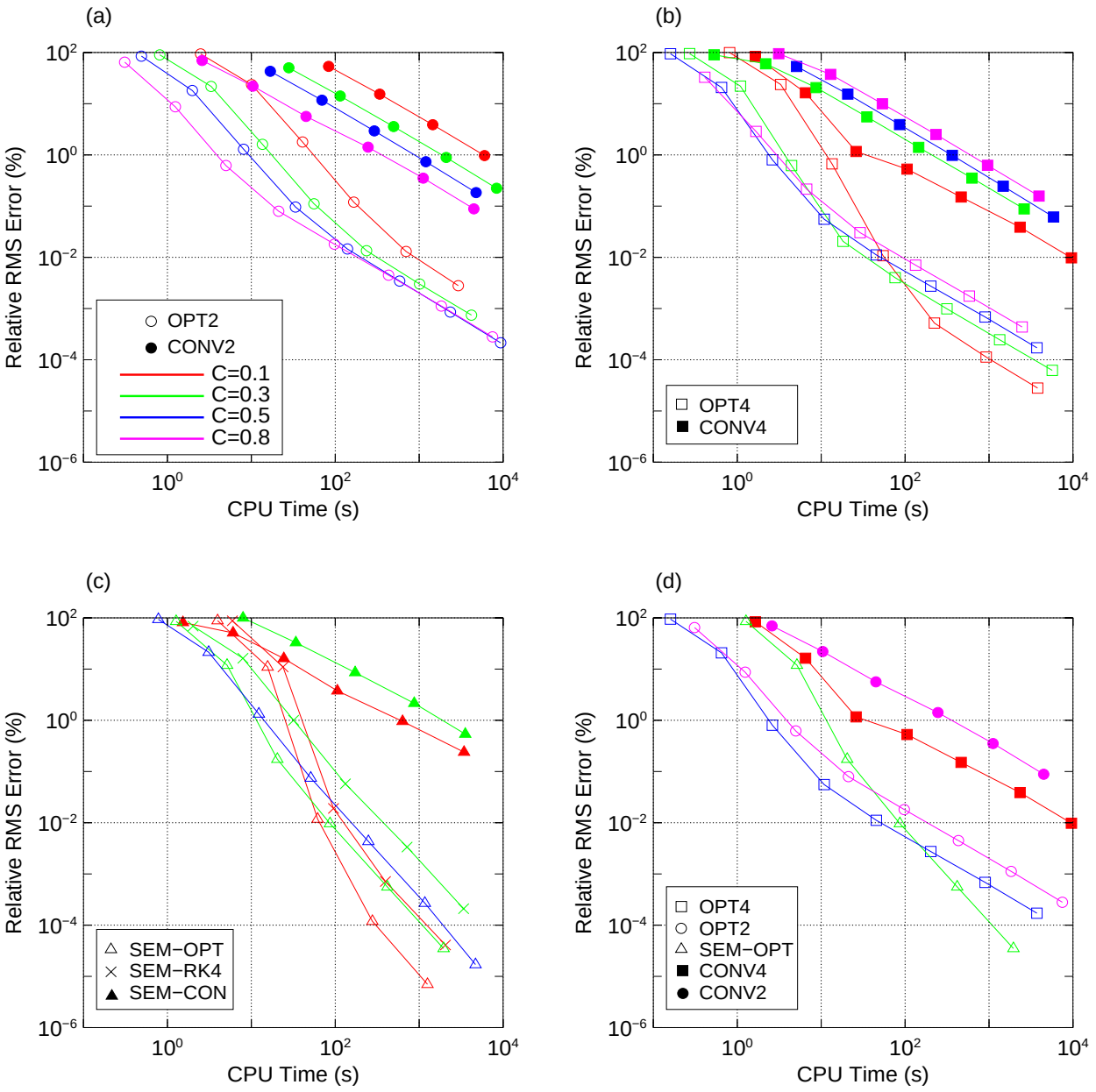

Figure 2. Relative r.m.s. error versus CPU time for Model A: (a) results for OPT2 and CONV2, (b) results for OPT4 and CONV4, (c) results for an SEM spatial scheme with various temporal schemes, (d) results for best performing schemes from each of the first three panels (see text for details), with CONV2 and CONV4 shown for comparison. The legends identifying the line colors used for each Courant number appear in panel (a), and are common to all four panels. Legends identifying the symbols for each scheme show only the schemes presented in that panel.

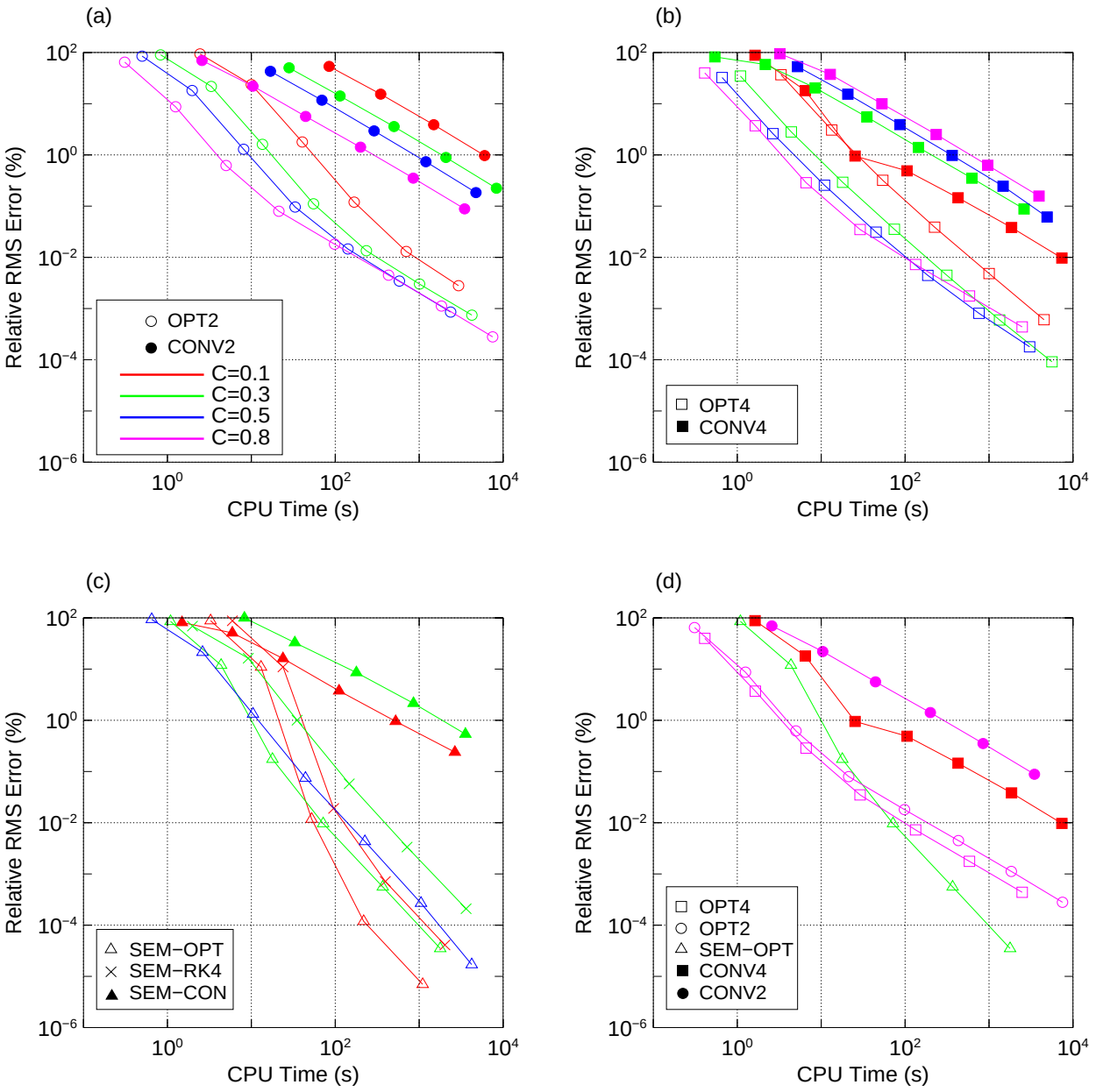

Figure 3. Relative r.m.s. error versus CPU Time for Model B. Display conventions are the same as in Fig. 2.

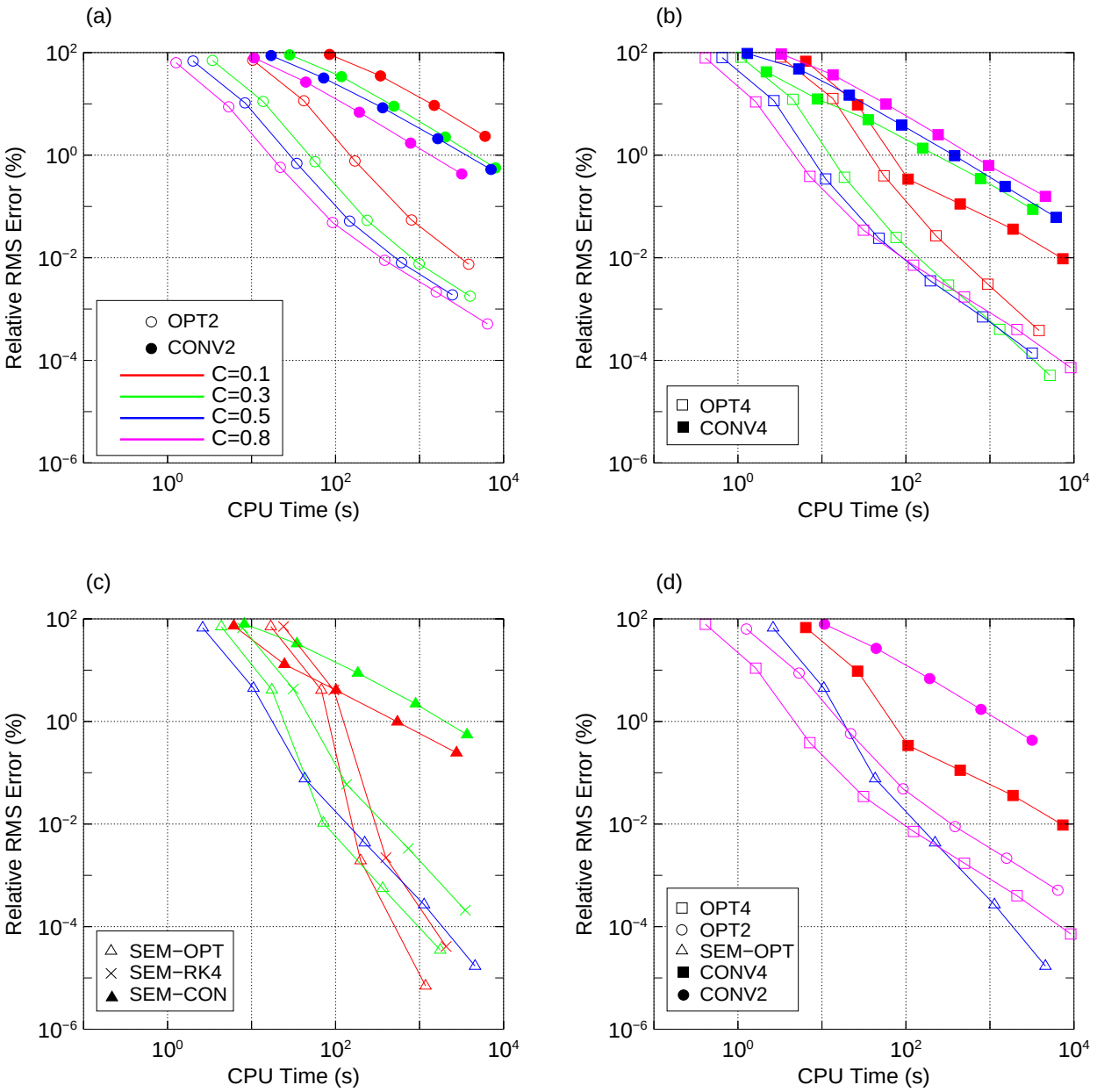

Figure 4. Relative r.m.s. error versus CPU Time for Model C. Display conventions are the same as in Fig. 2.

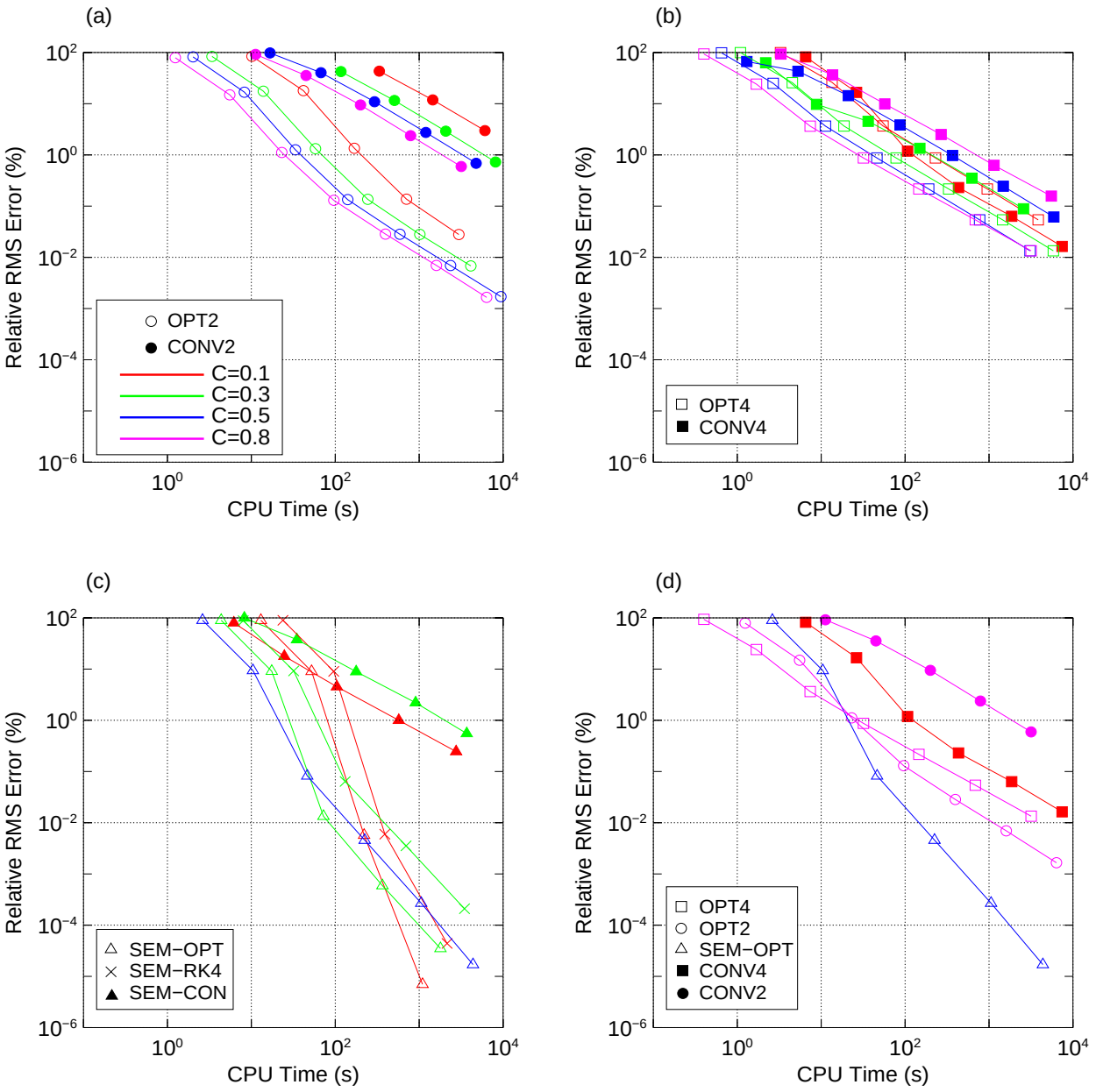

Figure 5. Relative r.m.s. error versus CPU Time for Model D. Display conventions are the same as in Fig. 2.

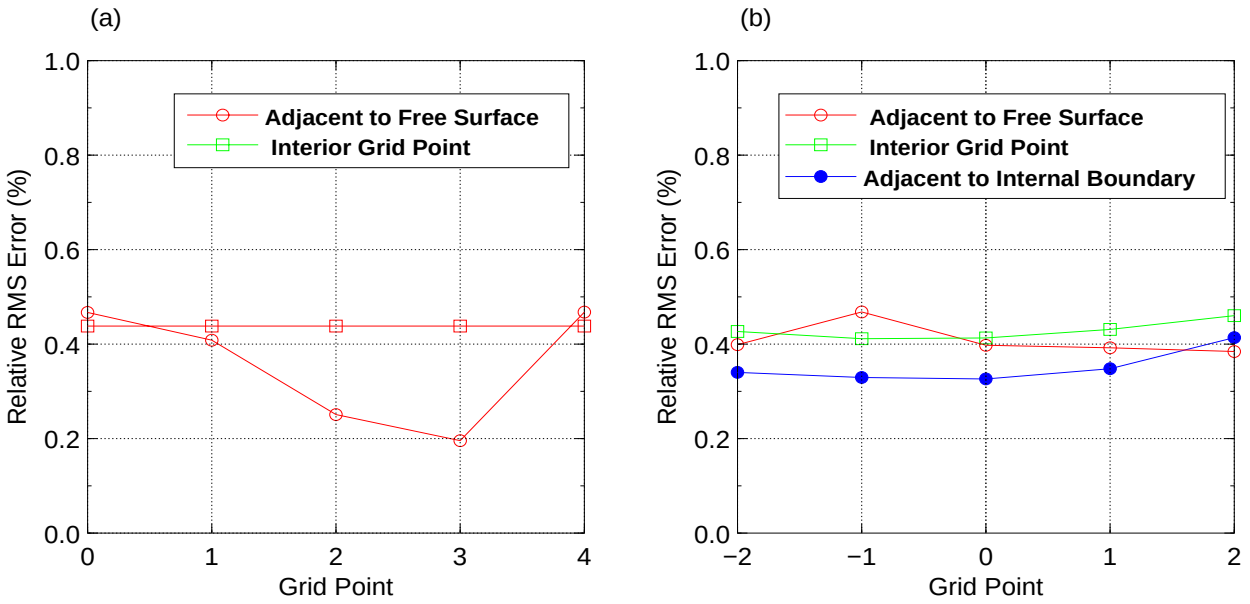

Figure 6. Relative RMS Error of OPT4 ($C = 0.5$) at grid points adjacent to the free surface at $x = 0$ km and at normal interior grid points around at $x = 1.125$ km for Model B (homogeneous model with free surface boundary conditions) with a grid spacing of $\Delta x = 0.03125$ km (left) and also at grid points adjacent to the internal boundary condition at $x = 0.75$ km for Model D (two-layer model with free surface boundary conditions) with a grid spacing of $\Delta x = 0.0078125$ km (right) respectively. Grid point at 0 represents the indicated position for the normal interior point and the internal boundary, and grid point at -2 represents the position of the free surface.

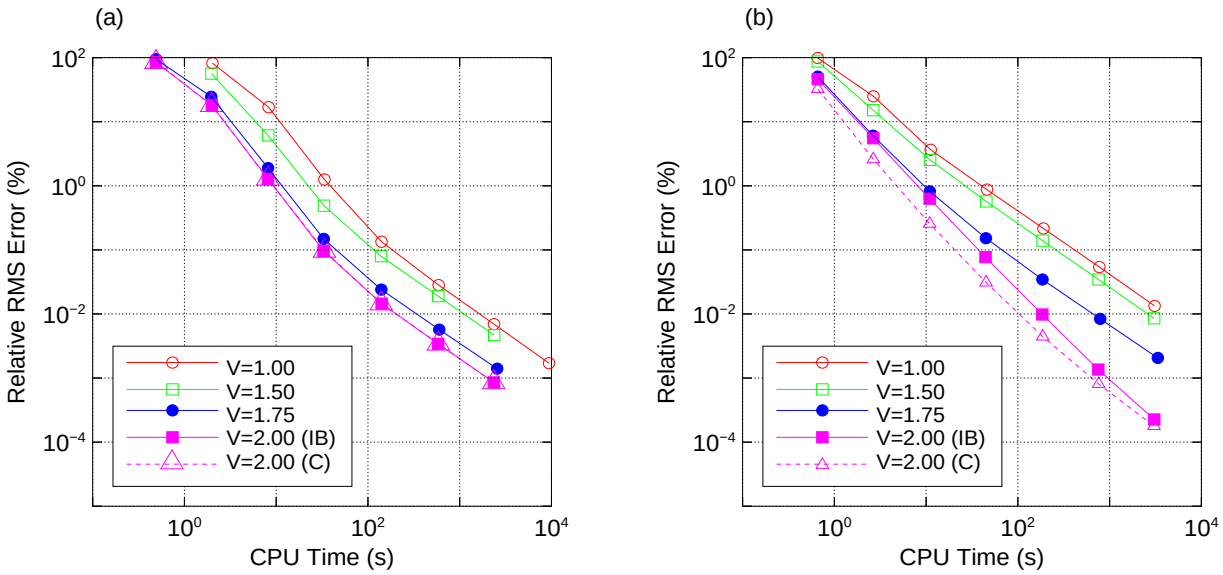

Figure 7. Relative r.m.s. error versus CPU Time results for various velocity value of the middle layer of Model D for (a) OPT2 and (b) OPT4 ($C = 0.5$). $v = 2.00$ (IB) and (C) represent a homogeneous model which contains boundary elements at the positions of layer boundaries and a homogeneous model which is only made up with normal elements respectively. The data points for (IB) and (C) for the case of $v = 2.00$ are perfectly overlaid in panel (a), which is expected because the two schemes are exactly equivalent.